Influence of Al/Si atomic ratio on optical and electrical properties of magnetron sputtered $Al_{1-x}Si_xO_y$ coatings

P. Costa[a], A. Al-Rjoub[a,*], L. Rebouta[a], N.K. Manninen[b], D. Alves[b], B. Almeida[a,c], N.P. Barradas[d], E. Alves[e].

a Centre of Physics, University of Minho, Campus de Azurém, 4800-058 Guimarães, Portugal
b Bosch Car Multimedia Portugal S.A., Rua Max. Grundig 35, Lomar, Braga, Portugal
c QuantaLab, University of Minho, Campus de Gualtar, 4710-057 Braga, Portugal
d Centro de Ciências e Tecnologias Nucleares, Instituto Superior Técnico, EN 10, km 139.7, 2695-066 Bobadela LRS, Portugal
e Campus Tecnológico e Nuclear, Instituto Superior Técnico, EN 10, km 139.7, 2695-066 Bobadela LRS, Portugal

* Corresponding author – e-mail address: abbaspl85@yahoo.com (A. AL-Rjoub)

Abstract

This work presents a study on the influence of the Al/Si atomic ratio in dc magnetron sputtered $Al_{1-x}Si_xO_y$ amorphous and transparent films upon their chemical composition, films' structure, optical and electrical properties. Increasing silicon in $Al_{1-x}Si_xO_y$ films, from 0 at. % up to 31.1 at. %, caused an increment of deposition rate and an increment in Al-O-Si energy bonds as confirmed by XPS analysis. On other hand, the optical constants (refractive index (n) and extinction coefficient (k)), dielectric constant, loss tangent (tan δ) and ac conductivity (σ_{ac}) decrease when the amount of silicon in films increased. The results show that refractive index varies linearly with volume % of Al_2O_3 (or SiO_2). Dielectric constant and dielectric loss evidenced two dipolar contributions, attributed to defects located one at or near the substrate/oxide interface, and the other in the bulk of the oxide.

Keywords: Sputtered $Al_{1-x}Si_xO_y$, Optical properties, Dielectric properties, Electrical conductivity.

1. Introduction

Recently, insulating SiO_2, Al_2O_3 and $Al_{1-x}Si_xO_y$ oxide layers have been used extensively in industrial applications, such as the optical applications and semiconductors devices, due to the combination of their transparency, diffusion barrier and electrical insulation properties. For example, $Al_{1-x}Si_xO_y$ and SiO_2 were used as antireflection layer in solar thermal absorber stacks, which also work as a protective barrier layer [1-3], SiO_2 and Al_2O_3 are widely used in electronic devices as thin film transistors, memories structure, tunnel diodes, and Si metal-oxide semiconductors [4-7]. Also, Al-SiO_2-(n or p) Si and $SiAlO_x$/p-Si are already used in manufacturing of some specific types of diodes, the so-called tunnel diodes Metal-Insulator-Semiconductor, which are used in microelectronics (memory devices, photo diodes) and in photo cells applications [8,9]. Using $Al_{1-x}Si_xO_y$ instead of SiO_2 or Al_2O_3 enables to have a combination between the properties of SiO_2 and Al_2O_3, which may improve the fracture toughness, corrosion and oxidation resistance. Also, silicon addition to Al_2O_3 films provides an optimal combination of breakdown field strength, band offset and dielectric constant [10]. Moreover, Al_2O_3 film defects, which result from the deviation of stoichiometry of Al and O atoms during the deposition, can be compensated by the addition of silicon to Al_xO_y films. $Al_{1-x}Si_xO_y$ films also contribute to the increment of the electrical resistivity of films and suppression of flat band shift and hysteresis on the C-V characteristics, as reported in [11]. Indeed, $Al_{1-x}Si_xO_y$ films exhibited no degradation in the leakage current compared with Al_2O_3 films and it can have better properties, while being deposited at lower temperatures, as compared with Al_2O_3. This degradation is explained by a formation of an interfacial layer when Al_2O_3 is deposited on Si substrate [12, 13]. So, using aluminum silicate ($Al_{1-x}Si_xO_y$) thin films enables to control the electrical and optical properties of those films by controlling their silicon composition. The silicon addition provides the possibility of controlling their dielectric constant to have the desired electrical and optical properties, which make them good candidates for insulating films for power devices and other optical applications [14]. Within the present work, the influence of variation of silicon amount in dc magnetron sputtered $Al_{1-x}Si_xO_y$ films upon their chemical composition, films' structure, optical and electrical properties were studied.

2. Materials and methods

2.1 Coatings deposition

Al_2O_3, $Al_{1-x}Si_xO_y$ and SiO_2 thin films were deposited by dc magnetron sputtered onto Si (100) wafer (used for Rutherford Backscattering Spectrometry (RBS), X-Ray Photoelectron Spectroscopy (XPS) and Scanning Electron Microscopy (SEM) analyses), glass (used for tracing the optical properties of films) and stainless steel (AISI304) substrates (used for Energy Dispersive X-ray Spectroscopy (EDS) analyses and for studying the electrical properties). The depositions were performed using a substrate holder placed 9 cm above the target and working in static mode. Al_2O_3 thin films were deposited using an aluminum target (99.99%) with a diameter of 10 cm and oxygen as reactive gas. The composition of Al and Si in $Al_{1-x}Si_xO_y$ films was varied by adding X number Si pellets uniformly distributed on the Al target erosion zone (X=2,3,5,9,11), each pellet with a diameter of 10 mm. The number of Si pellets is depicted in Table I, together with the coatings' thickness and chemical composition. A Si (100) wafer was used as a target for the deposition of SiO_2 coatings and oxygen as reactive gas.

The stainless steel and silicon substrates were cleaned ultrasonically with acetone for 15 min, and the chamber was evacuated to a base pressure of $2x10^{-4}$ Pa. In order to remove oxides and impurities from substrate surface, an etching step was performed before each deposition in an argon atmosphere (working pressure of 1.15 Pa) by applying a pulsed bias voltage of -500 V. For glass substrates, they were cleaned by alcohol only. The target was also sputter cleaned before each deposition in argon atmosphere (Ar flow of 50 sccm, resulting in a working pressure of 0.38 Pa) and by applying a current density of 6.4 mA/cm^2 for 3 min. During the target cleaning process, the substrates were protected by a stainless steel shield.

Table I – Coatings identification, chemical composition, thickness and deposition rate

Sample	**Number. of Si discs**	**Thickness (nm)**	**Deposition rate (nm/min)**	**Si (at. %)**	**Al (at. %)**	**Al/Si atomic ratio (EDS)**	**(Al+Si)/O atomic ratio (RBS)**
Al_2O_3	0	59.0	1.7	0	38.1	-	0.67
S2	2	375.9	10.7	29.9	6.6	4.52	0.57
S3	3	323.5	9.0	22.4	13.5	1.66	0.58
S5	5	387.1	11.0	11.4	23.1	0.49	0.54
S9	9	604.7	17.3	7.6	28.0	0.27	0.57
S11	11	751.3	21.5	4.6	31.1	0.15	0.58

The coatings were deposited in $Ar+O_2$ atmosphere, being the Ar and O_2 partial pressures of 0.38 Pa and 0.048 Pa, respectively. A current density of 6.4 mA/cm^2 was applied to the target. During deposition, a pulsed dc voltage of -60 V was applied to the substrate holder being the frequency 90 kHz. The deposition time was set to 35 min, and same deposition conditions were used for all reported thin films, being the only variable is the number of Si pellets.

2.2 Coatings' chemical composition, structure and morphology

The coatings' chemical composition was assessed by means of EDS and RBS analyses. Scanning electron microscopy analysis was performed in a NanoSEM-FEI Nova 200 (FEG/SEM) equipment, to determine the coatings thickness and morphology. EDS analysis allowed to determine the Al/Si atomic ratio, while RBS was used to assess the (Al+Si)/O atomic ratio. EDS analyses were performed with the electron beam of the SEM and a EDAX - Pegasus X4M system. The measurements were randomly performed on the sample surface with an acceleration voltage of 5 keV. RBS measurements were carried out at the CTN/IST Van de Graaff accelerator with detectors placed at 140º and 165º to the beam direction. Spectra were collected with a 2 MeV $^4He^+$ beam. Normal incidence was used in the experiments and the obtained data were analyzed with the IBA Data Furnace NDF v9.6i [15]. In order to evaluate the coatings' chemical bonding state X-Ray Photoelectron Spectroscopy (XPS) analysis was performed in a Kratos AXIS Ultra HAS X-Ray Photoelectron Spectroscopy system, using an Al Kα (1486.7 eV) X-Ray source, with a 40 eV pass energy. The C1s line at 285.0 eV was used to calibrate the binding energies. The XPS spectra were analyzed in CasaXPS software (version 2.3.19, Casa Softw. Ltd), and all peaks were fitted using a Shirley background and GL (30) line shape (GL (p): Gaussian/Lorentzian product formula where the mixing is determined by m = p/100, GL (100) is a pure Lorentzian while GL (0) is pure Gaussian.).

2.3 Optical and Electrical Characterization

The optical measurements, in transmittance and reflectance modes, were measured in the wavelength range of 250 – 2500 nm, using a Shimadzu PC3101 UV–VIS–NIR

scanning spectrophotometer. The reflectance measurements were performed at an incidence angle of 8º using an integrating sphere attachment and an Al mirror as a reference. The reflectance data were corrected according to the Al -reference reflectance curve. Then, the results were used to calculate the optical constants and thicknesses of films by using SCOUT software [16].

Capacitance – frequency (C-f) measurements, in the frequency range of 20 Hz – 3 MHz, were carried out at room temperature using the structure of Ag/ $Al_{1-x}Si_xO_y$ / Stainless steel, and the area of Ag electrode contact was calculated for each sample. The measurements were achieved using a WAYNE KERR 6440B precision component analyzer. The complex dielectric constant is given by $\varepsilon^*(\omega) = \varepsilon' - i\varepsilon''$, where ε' and ε'' are the real and imaginary parts, respectively. The dielectric loss is given by $\tan \delta = \varepsilon''/\varepsilon'$. So, the dielectric constant, the real part of the complex electric permittivity, was determined using the equation:

$$\varepsilon' = Cd/A\ \varepsilon_0. \qquad (1)$$

where C is the film capacitance, A is the surface area of the electrode, d is the thickness of film, and $\varepsilon_0 = 8.85 \times 10^{-12}$ F/m is the permittivity of vacuum.

The AC conductivity (σ_{ac}) of prepared films was calculated from the dielectric data using the equation [17]:

$$\sigma_{ac} = \varepsilon_0\ \varepsilon'\omega \tan \delta \qquad (2)$$

where ω is the angular frequency ($\omega = 2\pi f$, where f is the frequency of AC applied). The frequency dependent conductivity was determined from the universal power law [17]

$$\sigma(\omega) = \sigma\ (0) + B\omega^i \qquad (3)$$

where, σ (0) is the dc conductivity and $B\omega^i$ is the frequency dependent part of the conductivity with a factor B and frequency exponent $0 \leq i \leq 1$. The value of i was determined from the plot of $\ln(\sigma_{ac})$ vs $\ln(\omega)$ at high frequency [18-20].

3. Results and discussion

3.1 Definition of deposition parameters

The coating´s thickness and the deposition rate are summarized in Table I, together with Al/Si atomic ratio (determined from EDS analysis) and (Al+Si)/O atomic ratio

(obtained from RBS analysis). The coatings thickness was determined by SEM cross-sectional analysis, while the deposition rate was calculated by dividing the thickness by deposition time (35 min for all coatings). The coatings were labeled as S_X, where X represents the number of Si pellets incorporated in Al target erosion zone, e.g. S3 coating was deposited with 3 Si pellets placed on Al erosion zone. The Al_2O_3 coating, deposited without Si pellets and SiO_2 deposited without Al (not included in Table I, because was deposited with a Si target).

In order to attain transparent and dielectric coatings, it is necessary to guarantee that the deposition parameters allow having an adequate metal to oxygen ratio. In this sense, the first step was the setting of the deposition parameters with the main goal to fix all the deposition parameters, except for the amount of Si pellets in Al target. In the first step, the voltage-oxygen flow hysteresis curves were determined for different target conditions (amount of Si pellets) and different coatings were deposited at different points of the hysteresis plot in order to evaluate if transparent coatings were being obtained. The hysteresis curves of Al_2O_3 (reference coating without Si) and S9 coatings are depicted in Fig. 1.

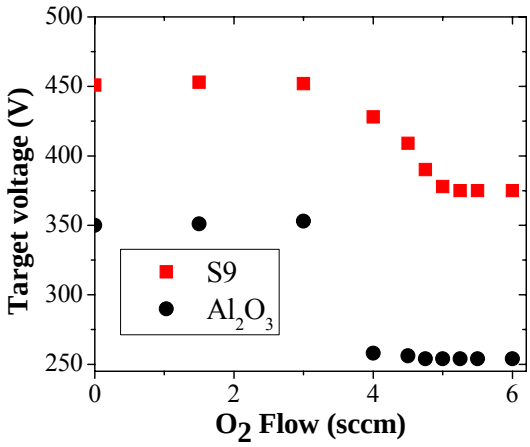

Fig. 1: The target voltage as a function of oxygen flow for Al_2O_3 (reference target) and sample S9.

The hysteresis curves indicate the variation of target voltage with reactive gas flow, which allows monitoring the target surface condition. Target surface poisoning in higher reactive gas flow can determine the coatings chemical composition as well as the deposition rate, since the oxidized target surfaces show a lower sputtering yield in relation to metallic targets, which leads to lower deposition rates in the reactive mode. The hysteresis curves shown in Fig. 1 indicate that the transition from metallic mode to transition mode occurs at 3 sccm for both targets, while the shift from transition mode to reactive mode occurred at 4 sccm and 5 sccm for Al_2O_3 and S9, respectively. This

indicates that the width of the transition zone is clearly larger for S9 as compared with Al_2O_3. Braeckman et al. [21] reported the variations in discharge voltage of Ti targets with Al rods in reactive sputtering, for different number of Al rods and different discharge currents. The authors observed a decrease in the transition width with the increase of number of Al rods, which was attributed to the higher ratio of the metal-to-metal (oxide) sputter yield (equivalent to higher deposition rate ratio of metal-to-metal(oxide)) of aluminum as compared to titanium. In the present work, a low transition width was observed in Al target, which is related to the high reduction in sputtering rate with the target surface oxidation, while for the S9 target the transition width increased, which is attributed to the lower reduction in sputtering yield of Si with oxidation. It would be expected that incorporation of Si pellets lead to a shift of the metallic to transition deposition mode to higher gas flow rate, nevertheless, for the oxygen flow steps used, this trend was not observed. The incorporation of Si pellets on Al target also promoted a shift of the hysteresis curves to higher voltage values, which is attributed to the changes in the secondary electrons emission yield with the incorporation of Si in Al target. For both Al and Si, it has been reported that the transition from metallic to reactive mode leads to a decrease in the target voltage [21]. All coatings were deposited in reactive mode for a gas flow rate of 0.048 Pa, being found that transparent coatings can be obtained.

3.2 Chemical composition and structure

The coatings' chemical composition was assessed by means of EDS and RBS analyses. EDS analysis allows to obtain better quantification of Al and Si allowing to determine the Al/Si atomic ratio; however, the oxygen quantification by means of EDS analysis is typically obtained with high error. In order to obtain a more accurate oxygen quantification the chemical composition was also assessed by means of RBS analysis, being the spectra of two coatings (S3 and S9) shown in Fig. 2. The relative heights of front edges of different elements (indicated in the figure) are correlated with the relative concentrations of those elements. The position of the different elements, located at surface sample, is indicated in the graph. Since the atomic masses of Al and Si are close, their quantification by means of RBS analysis leads to large uncertainties (around 3 to 5 at. %). However, the Si amount is higher on coating S9 when compared with the spectra of S3 coating. Thus, this characterization was used for the determination of (Al+Si)/O atomic ratio, which is shown in Table I. The spectra also show that sample

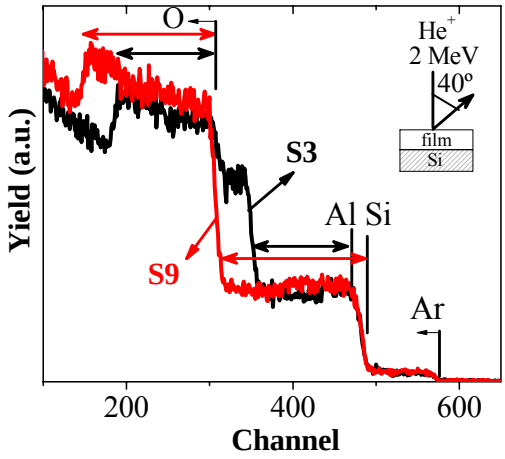

Fig. 2: RBS spectra of two different samples as varying the amount of silicon in films.

S9 is thicker than S3 sample, as previously described and shown in Table I. According to the RBS analysis the amount of oxygen in all coatings is nearly constant, showing values in order of 60 to 64 at.%. Regarding the Al and Si chemical composition the amount of Al decreases from 38.1 at. % (for reference Al_2O_3 coating) down to 4.6 at. % Al for S11 coating, while the Si content shows an opposite trend, increasing from 0 at. % for reference Al_2O_3 coating up to 31.1 at. % for S11 coating. Fig. 3 shows a fast increase in Si content when the number of silicon pellets is increased from 0 up to 5, which is accompanied by a fast decrease in aluminum content. However, increasing the number of silicon pellets from 5 up to 11 promotes a lower increase in the silicon content. In fact, this might be the saturation limit for Si, since at this chemical composition the Si:O is 1:2, which represents the stoichiometry of SiO_2. Regarding to the (Al+Si)/O atomic ratio, it can be found that this ratio is constant, showing an average value of 0.57, which is in between the Al/O atomic ratio for Al_2O_3 (0.67) and the Si/O atomic ratio for SiO_2 (0.5).

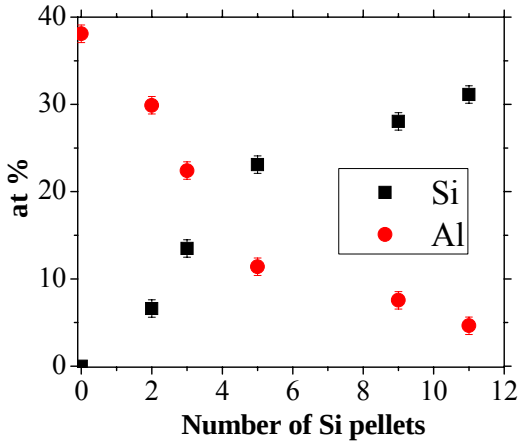

Fig. 3: Elemental composition of Si and Al in films as a function of silicon pellets as evaluated by EDS and RBS

For more details about the chemical structure, three samples: S3, S5 and S9 have been chosen for XPS analysis. Fig. 4 represents the evaluated XPS spectra of Al 2p and Si 2p core levels. As shown in Fig. 4a, the XPS spectra of Si 2p binding energy can be deconvoluted into two sub-peaks in all samples. The respective energies of 102.6 eV, 103.5 eV correspond to Al-O-Si and Si-O-Si, respectively [6,11,12,22-24]. The ratio of peak's areas (Al-O-Si /Si-O-Si) decreased with increasing silicon amount in films, which is 2.96, 1.72 and 0.82 for S3, S5 and S9, respectively.

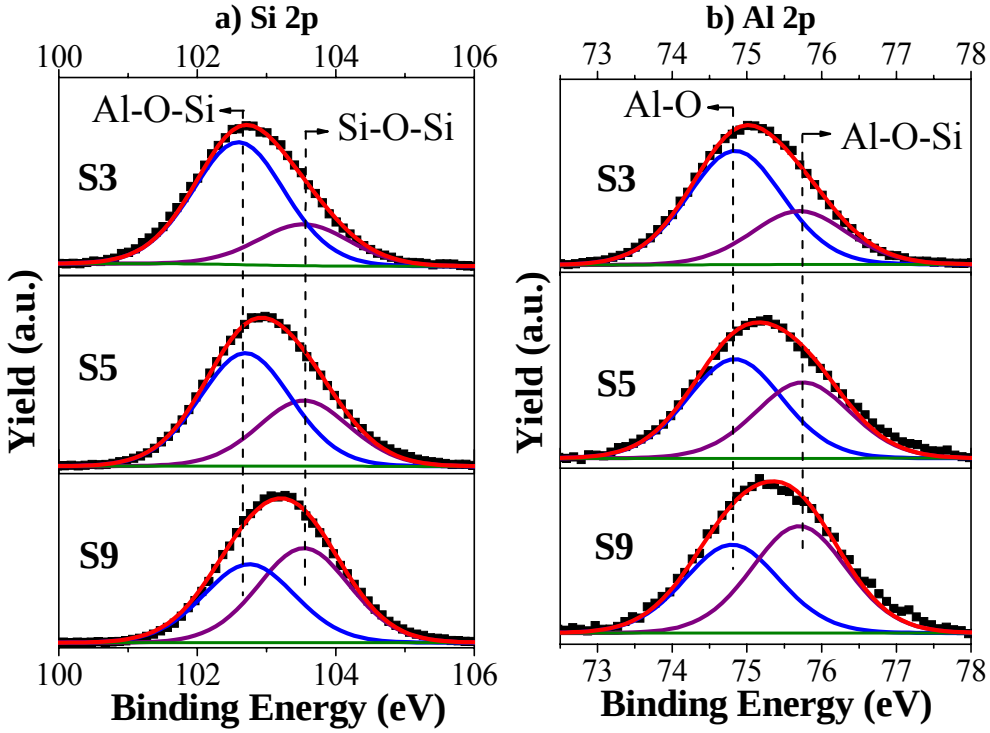

Fig. 4: XPS spectra of: (a) Si 2p and (b) Al 2p electrons for the three samples: S3, S5and S9. The green curve represents the background correction.

For Al 2p spectra, the spectra revealed two peaks located at 74.8 and 75.8 eV, as shown in Fig. 4b. The peaks at 74.8 eV and 75.4 eV are considered as Al-O and Al-O-Si compounds, respectively [11,12,24]. Moreover, peak's areas ratio (Al-O/Al-O-Si) have the same tend of decrement as in Si 2p spectra, with values 2.1, 1.3 and 0.83 for S3, S5 and S9, respectively. These results seem to indicate that Al(Si) is present as second neighbor of Si(Al) in relatively high percentage.

The grazing incident X-ray diffractograms for samples S3 and S9 are shown in Fig. 5, the spectra indicate that the coatings are amorphous. The SEM cross-sectional micrographs of S3 and S9 shown in Fig. 6 indicate that both coatings form a featureless morphology, which is the most typical morphology of amorphous coatings.

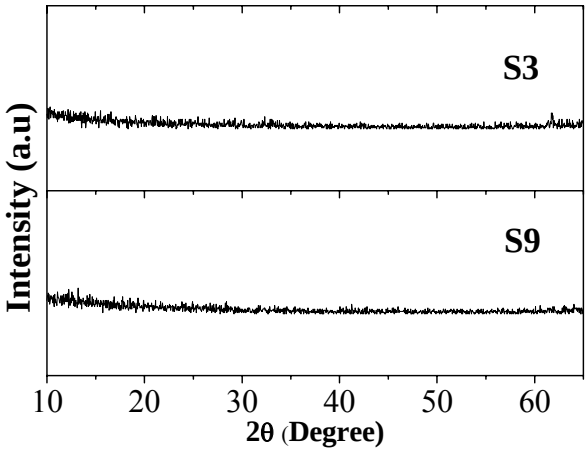

Fig. 5: X-ray diffraction spectra of samples S3 and S9.

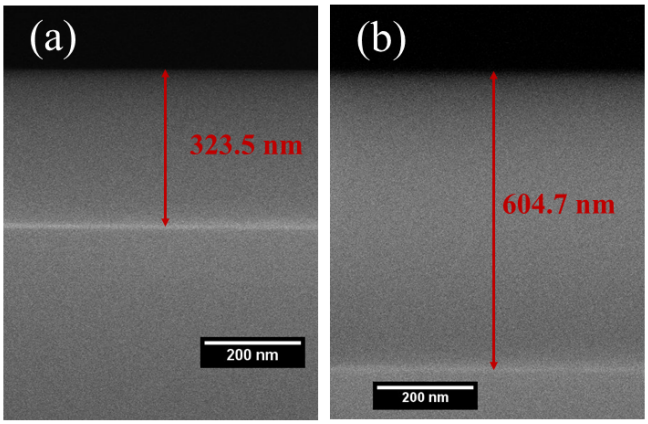

Fig. 6: Cross-sectional SEM micrographs show a compact featureless morphology of (a) S3 and (b) S9 samples.

3.3 Optical and electrical properties

Optical properties of these oxides are very important due to their high transmittance and low reflectance. This is associated with the low refractive index and almost zero extinction coefficient, which allow their use as antireflecting layer in several applications. All samples show a high transmittance and low reflectance. The reflectance decreases when the number of silicon discs in the target increases. The optical constants, refractive index (n) and extinction coefficient (k), were determined from the transmission (T) and the reflectance (R) curves [25] by using the optical simulation program SCOUT. As shown in Fig. 7a the addition of silicon is very noticeable, inducing the decrease of the refractive index. This behavior was expected since the refractive indices of silicon oxide and aluminum oxide are 1.48 and 1.68, respectively. So, the results indicate a general decrease of n and k as the amount of silicon is increased in films.

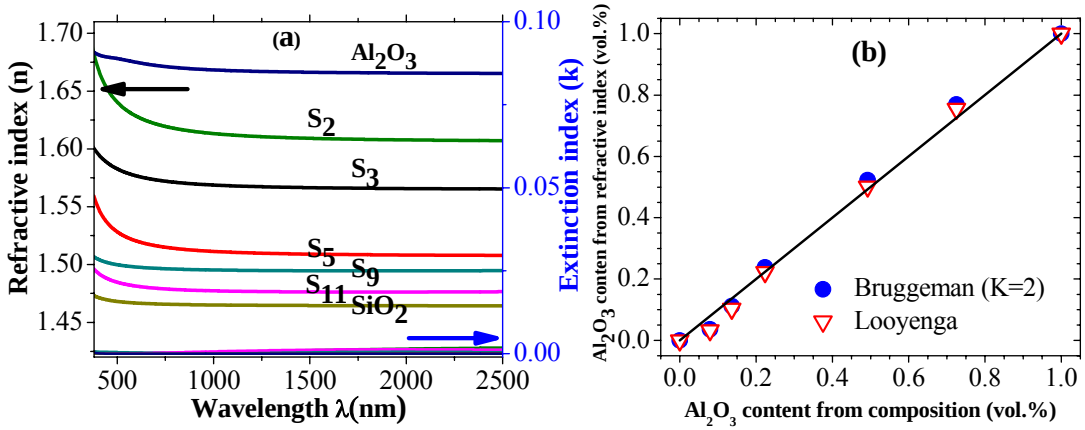

Fig. 7: (a) Refractive index (n) and extinction coefficient (k) of Al_2O_3, $Al_{1-x}Si_xO_y$ and SiO_2 as a function of wavelenght (λ), and (b) Volume contribution of Al_2O_3 phase estimated by Bruggeman and Looyenga effective medium approximation models as a function of the volume contribution of Al_2O_3 obtained from composition measurements. The straight line is only to guide the eyes and corresponds to case when the contributions are the same.

The refractive index of $Al_{1-x}Si_xO_y$ films was used to calculate the volume contribution of SiO_2 and Al_2O_3 phases, applying the Bruggeman effective medium approximation to estimate the contribution of each phase [26]:

$$f\frac{\varepsilon_A-\varepsilon_{eff}}{\varepsilon_A+K\varepsilon_{eff}}+(1-f)\frac{\varepsilon_B-\varepsilon_{eff}}{\varepsilon_B+K\varepsilon_{eff}}=0 \qquad (4)$$

where ε_A, ε_B and ε_{eff}, are the dielectric functions of Al_2O_3, SiO_2 and $Al_{1-x}Si_xO_y$ films, respectively, f and (1-f) are the volume contributions of Al_2O_3 and SiO_2 phases. K is a parameter that describes the topology of the constituents, and K=2 was used, which describes a volume that consists entirely of spherical particles of material A and B. In all cases the extinction coefficient is very close to zero and thus $\varepsilon=n^2$. The calculation was also performed with the theoretical model proposed by Looyenga [27] for heterogeneous mixtures and similar results were obtained:

$$\varepsilon_{eff}^{1/3} = f\,\varepsilon_A^{1/3} + (1-f)\varepsilon_B^{1/3} \qquad (5)$$

The results were drawn as a function of the volume contribution of Al_2O_3 and SiO_2 calculated from composition measurements (from Al and Si at.%, and using the densities expected for Al_2O_3 and SiO_2 amorphous phases of 3.2 g/cm^3 and 2.2 g/cm^3, respectively) and are presented in Fig. 7b. The results show that when the volume contribution of Al_2O_3 is lower than 22%, the Al_2O_3 volume contribution calculated from refractive index is lower than the one obtained from composition. On the other hand, when the volume contribution of Al_2O_3 is higher than 50%, the contribution calculated from refractive index is higher than one calculated from composition. These results suggest the presence of some Al atoms incorporated in SiO_2 when the volume

contribution of SiO_2 is higher than 78% (or Al_2O_3 vol.% lower than 22%), and some Si atoms incorporated in Al_2O_3 when the volume contribution of Al_2O_3 is higher than 50%, which agrees with the XPS analysis. This shows that the complete segregation of the Al_2O_3 and SiO_2 phases does not occur.

Mixtures with different composition can be used to deposit films with refractive indices in the range of 1.48 to 1.68. Additionally, a small Al addition to SiO_2 will increase slightly the refractive index, being still good for using as antireflection layer but with advantages during the deposition process and with good results in terms of protection against oxidation [1,28].

Frequency dependent capacitance (C-f) and loss tangent (tanδ) measurements were carried out at room temperature, in the frequency range of 20 Hz – 3 MHz, in order to determine the dielectric permittivity. As shown in Fig. 8a the dielectric constant, the real part of the complex permittivity, decreases with increasing the amount of silicon in the films. For example, the dielectric constant at 1 kHz decreased from 7.1, for Al_2O_3, to 3.9 for S11. Fig. 8b shows the dielectric loss tangent (tan δ) as a function of frequency at room temperature. Loss tangent gives the ratio of resistive or loss current to the charging current and it is directly related to ac conductivity. The measured values (Fig. 8b) indicate that these oxides are very good insulators.

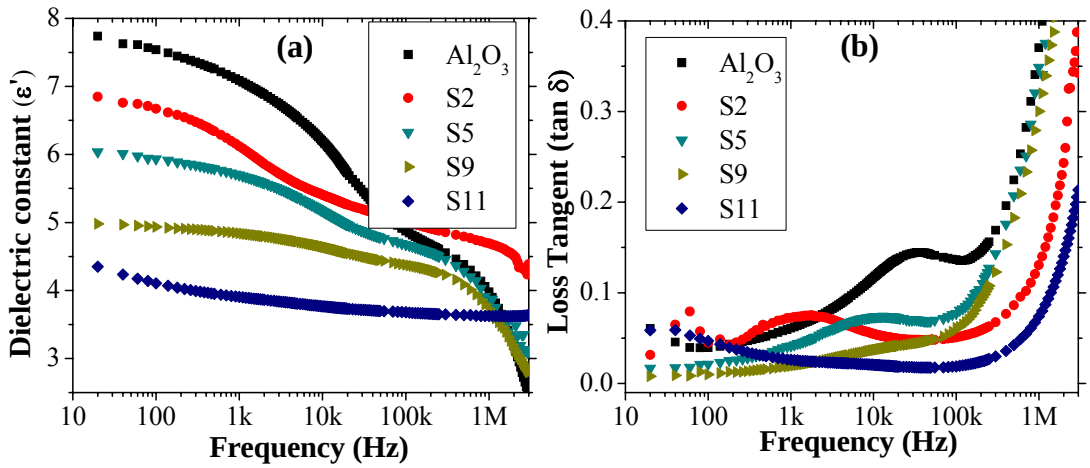

Fig. 8: a) Dielectric constant (ε′) as function of frequency and b) loss tangent (tan δ) as function of frequency.

The step like decrease in the dielectric constant as a function of frequency, ε′(f), corresponds to a relaxation process, with a characteristic relaxation time $\tau=1/(2\pi f)$ of the oscillating dipoles. The dielectric strength of the relaxation process can be determined from the step (Δε) in dielectric constant and it decreases with the increase of Si content, disappearing in sample S11, the sample with highest Si content. The peaks in dielectric

loss tangent correspond to this same relaxation process and its maximums occur at the same frequencies of the steps in the dielectric constant (Fig. 8a), and corresponding values are indicated in Table II. The frequencies at which these relaxations processes occur are in the range 1 - 36 kHz and, although their position is different for different Si concentration, due to different degree of Si dispersion in the films, their strength systematically decreases with increasing Si content. According to von Hippel [29] these peaks can be attributed to interface defects, which can be defects or traps, localized at, or near, the interface between the film and the substrate. The Maxwell–Wagner theory of a two-layer condenser [30] describes the interfacial space–charge polarization, which occurs at the interface of two contacting slabs of frequency-independent materials with significantly different conductivities and static dielectric constants. In the Al_2O_3 deposition, an interlayer usually forms at the interface between the oxide and substrate and the Si addition to Al oxide improves the interface quality [9, 10]. In this respect, the compensation created by the addition of silicon to Al_xO_y films [9,10,13] and the corresponding improvement of the interface quality leads to the decrease of defects and, thus, to the decrease of the dielectric strength of this interfacial contribution with the increase in Si content, as observed in our samples. The compensation effect is consistent with the results obtained by XPS and those shown in Fig. 7b obtained from volume contribution of SiO_2 and Al_2O_3 phases, applying the effective medium approximation models to estimate the contribution of each phase, where Al-O-Si bonds increased with Si content, indicating that Al(Si) is present as second neighbor of Si(Al) in relatively high percentage.

Table II – f_{max} of interfacial relaxation processes and exponent i for different silicon content in films

Sample	**f_{max} (kHz)**	**Exponent i**
Al_2O_3	35.2	0.66
S2	1.1	0.60
S5	13.8	0.55
S9	13.4	0.67
S11	-	0.54

A second step like decrease in the dielectric constant ε´(f), appears around 1-2 MHz and corresponds to the onset of a defect or dipolar relaxation peak that extends beyond the measured frequency range. They are usually associated to the presence of impurities

present in the structure, or traps that can be successively charged and discharged. Here, in particular, in this frequency region this relaxation can be associated with Maxwell-Wagner space-charge interfacial effects occurring at Al_2O_3-SiO_2 interfaces [31] as a result of the dispersion of the silicon in the alumina matrix.

The dielectric constant at 1 kHz, as a function of Al_2O_3 vol%, is represented in Fig. 9 for the different samples. The dielectric constant increases with Al content, but in the range from 14 to 22 Al_2O_3 vol% (7.6 to 11.4 Al at.%) its values increase faster due to percolation [32] . As shown in Fig. 7b, this is also the composition region where the Al_2O_3 phase contribution for refractive index is lower than one calculated from composition, suggesting that some Al atoms are incorporated in SiO_2 phase. A similar effect was seen in resistivity with increasing Si content [9], in the region between 50 and 65 vol% of Al_2O_3 (from 9 to 13 Si at.%), but not seen in our samples composition. (we don´t have enough samples in that range), and it is also a composition region where the SiO_2 phase contribution for refractive index (Fig. 7b) is lower than one calculated from composition.

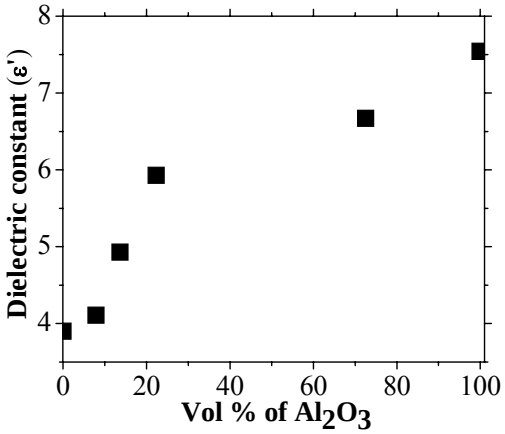

Fig. 9: Dielectric constant as a function of the Al_2O_3 vol%.

The Cole/Cole plots (or Argand plot) of the dielectric spectra are represented in Fig. 10, where the imaginary part of the complex permittivity, ε´´(ω), is plotted as a function of the corresponding real part, ε´(ω). The curves consist of a double arc, which represent the two relaxation regions, being the left arc the relaxation behaviour of the Maxwell-Wagner dipole polarization of film and the right arc the space charge polarization due to the previously referred film-substrate interfacial defects. The radius of the arcs (Δε) is the dielectric strength of the relaxation process. The right arcs show a depressed structure, having the high and low frequency sides with different tilt, indicating an

asymmetric distribution of relaxation times [17], related to the degree of homogeneity of the Si dispersion near the interface [31].

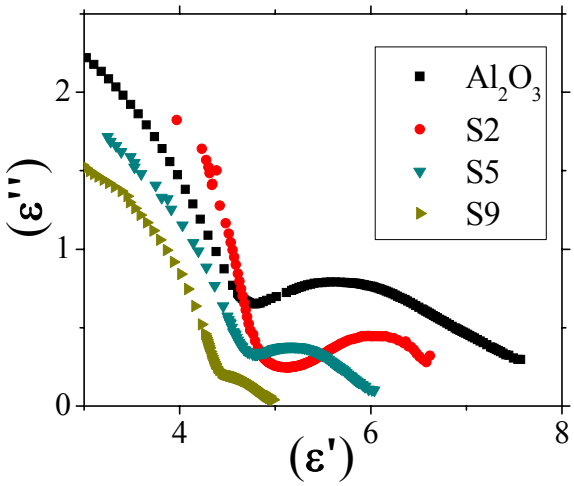

Fig. 10: Cole/Cole plots (ε'' as a function of ε').

For the frequency dependent conductivity, Fig. 11 shows the plotting of ln (σ_{ac}) vs. ln(ω), which is used to evaluate the frequency exponent i, from equation (3). The conductivity decreases with increasing silicon content and the lowest obtained value is for S11 (i.e at the frequency of 9 kHz the ac conductivity of Al_2O_3 was 9.8 $\times 10^{-9}$ S/m and it decreased to 3.9 $\times 10^{-9}$ S/m for S11). The Si addition leads to an improvement of the electrical insulation. The fitted i values are presented in Table II, and as seen, they are between 0.54 and 0.67, which are characteristic of disordered solids, where $0.5 < i < 1$ [32, 33], as in the case of the amorphous films studied here. The i values in this range are associated with hopping conduction mechanisms [32].

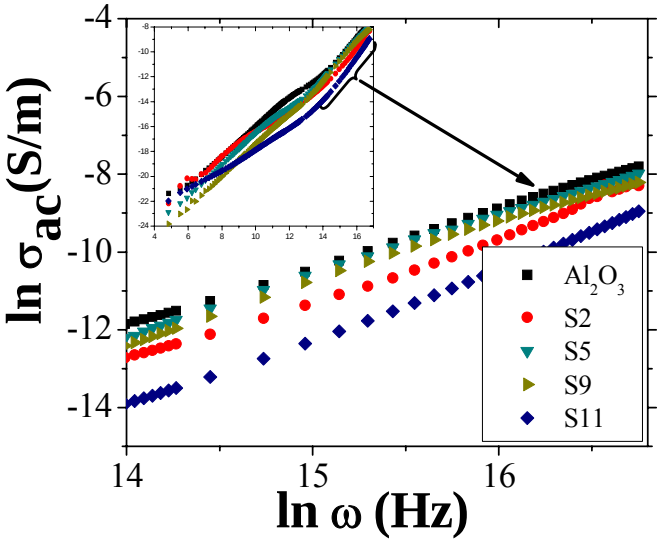

Fig. 11: ln (σ_{ac}) as a function of ln (ω).

4. Conclusions

The influence of variation of Al/Si atomic ratio on dc magnetron sputtered $Al_{1-x}Si_xO_y$ coatings chemical composition, structure, optical and electrical properties were studied. The partial pressure of the oxygen as reactive gas (0.048 Pa) was sufficient for oxidation leading to the formation of transparent films, being found that the deposition rate of these oxides increased with increasing the silicon amount in coatings, from 0 at. % up to 31.1 at. %. All coatings are amorphous as confirmed by XRD and showing a compact and featureless morphology typical from amorphous coatings, according to the SEM analysis. The Al/Si atomic ratio was varied from 4.52 down to 0.15, through the variation of Al/Si erosion area ratio in the sputtering target, while the oxygen amount was nearly constant leading to an (Al+Si)/O atomic ratio of 0.54 to 0.58 in $Al_{1-x}Si_xO_y$ coatings. The XPS analysis allowed to identify the binding state of the coatings, being observed that all coatings contain Si-O-Si, Al-O-Si and Al-O-Al bonds, being the contribution of each phase dependent on the amount of Al and Si in coatings, with the contribution of Al-O-Al bonds increasing with Al/Si atomic ratio while the contribution of Si-O-Si decreases. The transmittance of oxides layers increases (reflectance decreases) as increasing silicon and showing general behavior of decrement of the optical constant n and k.

The dielectric function of $Al_{1-x}Si_xO_y$ films was used to calculate the volume contribution of SiO_2 and Al_2O_3 phases, applying effective medium approximation models to estimate the contribution of each phase. The results show that when the volume contribution of Al_2O_3 is lower than 22%, the Al_2O_3 volume contribution calculated from dielectric function is lower than one obtained from composition. On the other hand, when the volume contribution of Al_2O_3 is higher than 50%, the contribution calculated from refractive index is higher than one obtained from composition.

Finally, the calculated dielectric constant, tangent loss and ac conductivity of the films are also decreased as increasing silicon in films, which mean that those oxides are good electrical insulators and good candidates for some electrical and optical applications. Dielectric constant and dielectric loss evidenced two dipolar contributions, attributed to defects located one at or near the substrate/oxide interface, and the other in the bulk of the oxide. The dielectric constant at 1 kHz in the range from 14 to 22 Al_2O_3 vol% (7.6 to 11.4 Al at.%) increases faster, what coincides with the composition region where the Al_2O_3 phase contribution calculated from dielectric function is lower than one

calculated from composition, suggesting that some Al atoms are incorporated in SiO_2 phase.

ACKNOWLEDGMENTS

The authors acknowledge the support of FCT in the framework of the Strategic Funding UID/FIS/04650/2013 and the financial support of FCT, POCI and PORL operational programs through the project POCI-01-0145-FEDER-016907 (PTDC/CTM-ENE/2892/2014), co-financed by European community fund FEDER. The authors also acknowledge the support of the European Structural and Investment Funds in the FEDER component, through the Operational Competitiveness and Internationalization Programme (COMPETE 2020) [Project nº 002814; Funding Reference: POCI-01-0247-FEDER-002814].

References

[1] L. Rebouta, A. Sousa, M. Andritschky, F. Cerqueira, C.J. Tavares, P. Santilli, K. Pischow, Solar selective absorbing coatings based on AlSiN/AlSiON/AlSiOy layers, Appl. Surf. Sci. 356 (2015) 203–212.

[2] A. Al-rjoub, L. Rebouta, P. Costa, N.P. Barradas, E. Alves, P.J. Ferreira, K. Abderra, A. Matilainen, K. Pischow, A design of selective solar absorber for high temperature applications, Sol. Energy. (2018).

[3] A. AL-Rjoub, L. Rebouta, P. Costa, L.G. Vieira, Multi-layer solar selective absorber coatings based on W/WSiAlN x\WSiAlOyNx /SiAlOx for high temperature applications, Sol. Energy Mater. Sol. Cells. 186 (2018) 300–308.

[4] J. Lu, C. Gong, X. Ou, W. Lu, J. Yin, B. Xu, Y. Xia, Z. Liu, A. Li, The roles of the dielectric constant and the relative level of conduction band of high-k composite with Si in improving the memory performance of charge-trapping memory devices, AIP Adv. 4, 117110 (2014).

[5] A. Bouazra, S.A. Nasrallah, M. Said, A. Poncet, Current Tunnelling in MOS Devices with Al2O3/SiO2 Gate Dielectric, Res. Lett. Phys. 2008 (2008).

[6] S. Heo, M. Chang, Y. Ju, S. Jung, H. Hwang, The effect of KrF laser annealing within an ultrashort time on metal-alumina-nitride- oxide-silicon-type flash memory devices, Appl. Phys. Lett. 93, 172115 (2008).

[7] R. Brendel, R. Hezel, Infrared observation of activated oxide reduction within Al/SiOx/ Si tunnel diodes, J. Appl. Phys. 71, 4377 (1992).

[8] J. Vuillod, G. Pananakakis, Electronic properties of Al-SiO2- (n or p) Si MIS tunnel diodes, Rev. Phys. Appl. 20 (1985) 33–44.

[9] E.T. Benny, J. Majhi, Tunnel oxides in AlSiOx /p-Si diodes by high pressure, low temperature oxidation of Si(100) and Si(111), Semicond. Sci. Technol. 7 (1992) 154–159.

[10] C. Gupta, S.H. Chan, A. Agarwal, N. Hatui, S. Keller, U.K. Mishra, First demonstration of AlSiO as gate dielectric in GaN FETs□; applied to a high performance OG-FET, IEEE Electron Device Lett. 3106 (2017).

[11] N. Komatsu, K. Masumoto, H. Aoki, C. Kimura, T. Sugino, Characterization of Si-added aluminum oxide (AlSiO) films for power devices, Appl. Phys. Lett. 256 (2010) 1803–1806.

[12] T.M. Klein, D. Niu, W.S.E. Li, D.M.M.C. Hobbs, R.I.H.J.R.B. N, Evidence of aluminum silicate formation during chemical vapor deposition of amorphous thin films on Si (100), Appied Phiscs Lett. 75, 4001 (1999).

[13] M. Copel, E. Cartier, E.P. Gusev, S. Guha, N. Bojarczuk, M. Poppeller, Robustness of ultrathin aluminum oxide dielectrics on Si (001), Appied Phiscs Lett. 78,2670 (2001).

[14] J.W. Lim, J. Yun, J.H. Lee, Electrical Properties of Aluminum Silicate Films Grown by Plasma Enhanced Atomic Layer Deposition, Electrochem. Solid-Ssate Lerrers. 9 (1) F8-F (2006).

[15] N.P. Barradas, C. Jeynes, Advanced physics and algorithms in the IBA DataFurnace, Nucl. Instruments Methods Phys. Res. B. 266 (2008) 1875–1879.

[16] W. Theiss, SCOUT Thin Film Analysis Software Handbook, (2002).

[17] F. Kremer, A. Schönhals, Broadband Dielectric Spectroscopy, Springer-Verlag, Berlin, 2003.

[18] K.C. Kao, Dielectric Phenomena in Solids, 1st ed., Academic Press, London, 2004.

[19] K.J. Hamam, M.M. Al-amar, G. Mezei, R. Guda, C. Burns, High dielectric constant response of modi filed copper phthalocyanine, J. Mol. Liq. 199 (2014) 324–329.

[20] S.I.S. Ramya, C.K. Mahadevan, S.T.H. College, Effect of calcination on the electrical properties and quantum confinement of fe2O 3 nanoparticles, Int. J. Res. Eng. Technol. 3 (2014) 570–581.

[21] B.R. Braeckman, F. Boydens, D. Depla, D. Poelman, Reactive sputter deposition of Al doped TiOx thin films using titanium targets with aluminium inserts, J. Alloys Compd. 578 (2013) 44–49.

[22] Y. Huang, S. Lv, X. Tian, R.K.Y. Fu, P.K. Chu, Interface analysis of inorganic films on polyimide with atomic oxygen exposure, Surf. Coat. Technol. 216 (2013) 121–126.

[23] J. -W. He, X. Xu, J.S. Corneille, X-ray photoelectron spectroscopic characterization of ultra-thin silicon oxide films on a Mo (100) surface, Surf. Sci. 279 (1992) 119–126.

[24] O.N.J. Hartmann, A.J. Hartmann, Influence of interface and Al structure on layer exchange during aluminum-induced crystallization of amorphous silicon, J. Appl. Physiscs. 88, 716 (2000).

[25] M. Fox, Optical properties of solids, Oxford university press Inc., NewYork, Oxford, 2001.

[26] D. A. G. Bruggeman, Berechnung verschiedener physikalischer Konstanten von heterogenen Substanzen, Ann. Phys. 24 (1933) 633.

[27] H. Looyenga, Dielectric constants of heterogeneous mixtures, Physica. 31 (1965) 401–406.

[28] D. Dias, L. Rebouta, P. Costa, A. Al-rjoub, M. Benelmeki, C.J. Tavares, N.P. Barradas, E. Alves, P. Santilli, K. Pischow, Optical and structural analysis of solar selective absorbing coatings based on AlSiOx□:W cermets, Sol. Energy. 150 (2017) 335–344.

[29] A. Von Hippel, A.S. Labounsky, Dielectrics and waves, Artech House Publishers, United States, 1995.

[30] N. Clément, S. Pleutin, D. Guérin, D. Vuillaume, Relaxation dynamics in covalently bonded organic monolayers on silicon, Phys. Rev. B. 82, 035404 (2010).

[31] B.D. Bertram, R.A. Gerhardt, Effects of Frequency, Percolation, and Axisymmetric Microstructure on the Electrical Response of Hot-Pressed Alumina–Silicon Carbide Whisker Composites, Am. Ceram. Soc. 94 [4] (2011) 1125–1132.

[32] J.C. Dyre, T.B. Schrøder, Universality of ac conduction in disordered solids, Rev. Mod. Phys. 72 (2000) 873–892.

[33] J.C. Dyre, A simple model of ac hopping conductivity in disordered solids, Phys. Lett. 108A (1985) 457–461.